#### SEISMIC PERFORMANCE OF BRIDGES WITH PIER WALLS

Shi Qi W. Wang, Tracy C. Becker

Department of Civil and Environmental Engineering University of California, Berkeley

#### **Abstract**

Pier walls used in highway bridge overpasses typically are squat shear walls with a height to width ratio lower than two. Squat walls are characterized by brittle shear failure modes. Unlike squat walls used in buildings, bridge pier walls have different reinforcement amounts, detailing, and loading demands, which affect the wall's strength and ductility. Three large scale squat shear wall experiments have been tested to better understand the failure mechanism and behavior of bridge pier walls. All specimens had an ultimate drift exceeding 1.5% and saw sliding shear failure. CSMIP sensor data of a squat pier wall bridge is also analyzed to better understand the relationship between a component pier wall model and a global bridge system model.

### Introduction

Reinforced concrete pier walls are typically used as bridge pier supports over waterways or as an alternative to typical reinforced concrete columns. Due to the geometry of the highway bridge, these walls are typically squat, with a typical height to width aspect ratio below 1.5. As squat shear walls primarily resist lateral seismic forces through brittle shear action, current design provisions (California Department of Transportation, 2019) are highly conservative, which in conjunction with capacity design, drives up the design cost of all connected members including the foundation.

Despite the multitude of squat shear wall experiments in existing literature (Gulec & Whittaker, 2009; Abo-Shadi et al., 2000; Haroun et al., 1994), the majority are for building walls rather than those used in bridges. There are three main factors that distinguish pier walls from the more commonly studied building walls. First, these pier walls typically have uniformly distributed steel reinforcement without any concentrated steel in the boundary elements, and also make use of crossties which are rarely seen in building walls. Second, pier walls serve as the primary lateral resisting system both along the wall strong and weak direction unlike building walls where perpendicular sets of shear walls are common. The influence of bidirectional loading can increase damage and reduce the ductility compared to unidirectional loading. Lastly, the vertical reinforcement ratio typically used in the pier walls is around 0.5%, lower than those typical in building walls. This reduces the flexural strength of the wall and can lead to more ductile flexure or flexure-shear failure modes, even in a squat wall.

There are numerous failure mechanisms possible for squat shear walls, all of which should be considered to accurately predict the response for any given wall. These include a

diagonal compression failure due to concrete crushing along a diagonal strut, diagonal tension failure due to insufficient horizontal reinforcement, sliding failure along the wall-footing interface, and flexure and flexure-shear combined failure modes. Consequently, due to both the detailing and loading differences, as well as the complicated failure mechanisms, purely analytical modelling of these particular shear walls is insufficient to inform how they should be designed.

This paper presents an overview of the first set of three bridge pier wall experiments conducted at UC Berkeley, preliminary pier wall modelling, and data investigation of a pier wall bridge instrumented with CSMIP sensors.

# **Experimental Tests**

In conjunction with Caltrans, an experimental program is currently underway and three large scale pier wall specimens have been tested in the structures laboratory at UC Berkeley. The reinforcement and detailing of the specimens was representative of typical current Caltrans design and all three specimens had nominally the same design while the loading protocol was varied.

# **Test Specimens**

The experimental reinforced concrete pier walls were 1:3 scale and were designed based on a typical Caltrans pier wall, with reinforcement details seen in Table 1. The specimens were 9.5 feet wide, 7 feet tall, and 9 inches thick and had two curtains of horizontal and vertical reinforcement, as shown in Figure 1. Crossties were placed at every vertical and horizontal bar intersection and the horizontal bars in the bottom 24 inches of the wall (plastic hinge region (PH)) were also hooked. The horizontal bars were closely spaced within the plastic hinge, as is typical of current Caltrans detailing requirements. The specimen reinforcement layout was scaled to maintain similar PH confinement ratios as those of the prototype wall. Typical concrete cover of 1 inch and 3.5 ksi strength Portland cement concrete with a nominal aggregate size of 3/4 inches was used.

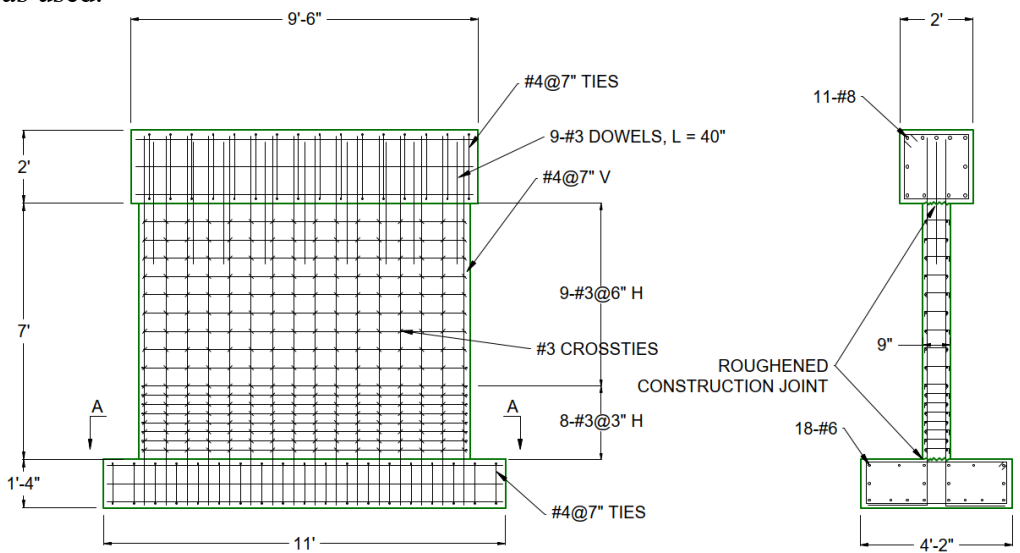


Figure 1. Typical specimen reinforcement and detailing.

**Table 1.** Specimen Reinforcement Details

Vertical Reinforcement	Horizontal Reinforcement	Crosstie Reinforcement	
#4 at 7"	Hooked #3 at 3" in the PH. #3 at	#3 hooked 135° and 90° ties at	
	6" otherwise.	every intersection.	
$\rho = 0.63\%$	$\rho = 0.81\%$ in PH	$\rho = 0.52\%$ in PH	

# **Loading Protocol**

The specimens were loaded in a cyclic quasi-static load protocol. For each load stage, the specimen was cycled at some displacement target, which was then increased upon completion of the load stage. A constant axial gravity load of 100 kips (2.8% axial load ratio) was applied and maintained on all specimens throughout the testing with prestressed rods and hydraulic jacks.

The first specimen was loaded purely unidirectionally in the strong direction and at each displacement target load stage, the specimen was cycled, as shown in Figure 2. For drifts less than 0.2%, the specimen was cycled three times while at drifts beyond 0.2% the specimen was only cycled twice. Each displacement target was increased by 1.33-1.50 times the previous cycle.

The remaining two specimens were tested with bidirectional loading protocols. The load protocols were developed based on the large difference in relative stiffness between the strong (in-plane) and weak axis (out-of-plane) of the wall. As the strong axis is stiffer than the weak axis, vibration in the weak axis has a longer period. During one displacement excursion in the more flexible direction, the wall would likely vibrate multiple times in the stiffer direction. To represent this, the chosen load pattern first cycles the wall in the strong axis with no weak axis displacement, and then adds weak axis displacement, as shown in Figure 3. This weak axis displacement is held constant while the wall is further cycled once more in the strong direction, and then the weak axis displacement is reduced to zero with the strong axis displacement at zero. Upon returning to zero total displacement, the displacement targets are increased for the next load stage and the weak axis displacement direction is also changed for the next load stage. For the second wall, a ratio of 4:1 weak axis to strong axis displacement target (based on the ratio of yield displacements in the hysteresis from test 1 and those from a flexural analysis of the wall in the weak direction) was used.

To determine the most appropriate load orbit for the third test, a non-linear single degree of freedom dynamic analysis was conducted on a suite of ground motions using Bispec (Earthquake Solutions, 2009). The relative strong and weak axis stiffnesses and yield drifts as measured from the second test (shown in Figure 4) were used to approximate a bilinear backbone curve for the model's strong and weak direction. A simple abutment model (California Department of Transportation, 2019) was added to the wall stiffnesses in both directions as shown in Figure 5. It was found that the displacement demand in the weak direction was a minimum of 4 times greater than that in the strong direction, and often significantly larger as shown in Figure 6. As a result, the third specimen loading protocol was similar to that of the second, except the ratio of weak to strong axis displacement was increased from 4:1 to 8:1. Similar ratios to these are found when looking at the CSMIP data from a pier wall bridge which will be discussed later.

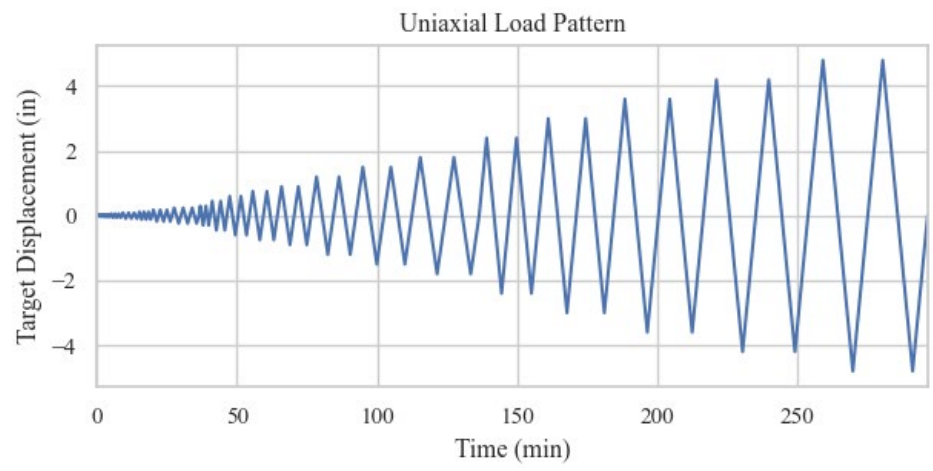


**Figure 2.** Example uniaxial test loading protocol. The specimen was held at the first peak displacement during each cycle to mark cracks.

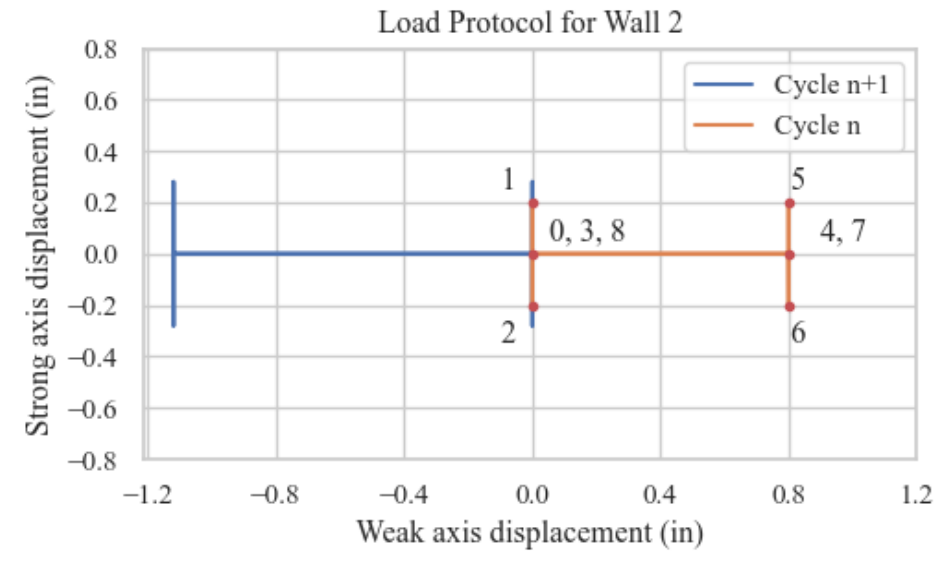


**Figure 3.** Bidirectional load protocol orbit. The points are ordered by increasing numbers. The next cycle will push the weak axis in the alternating direction.

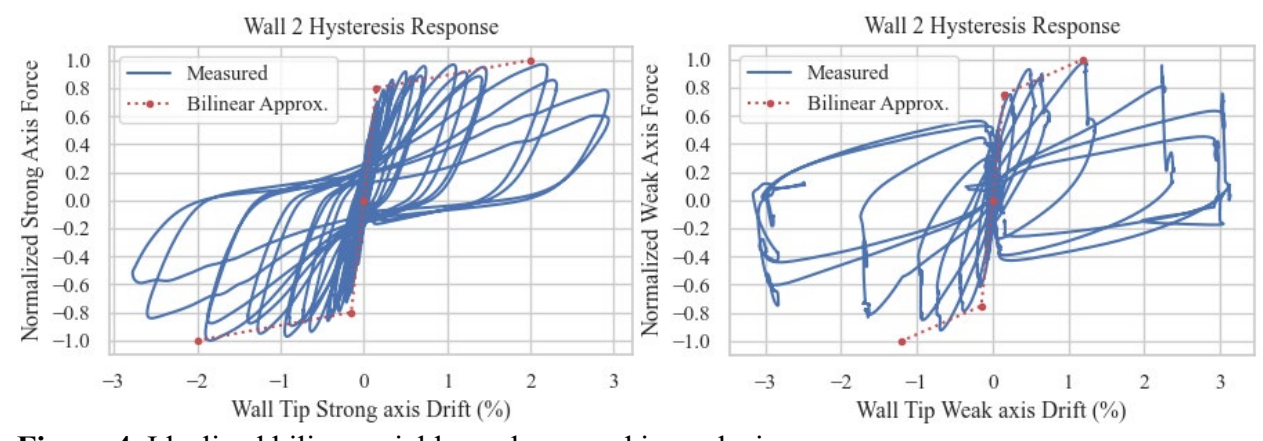
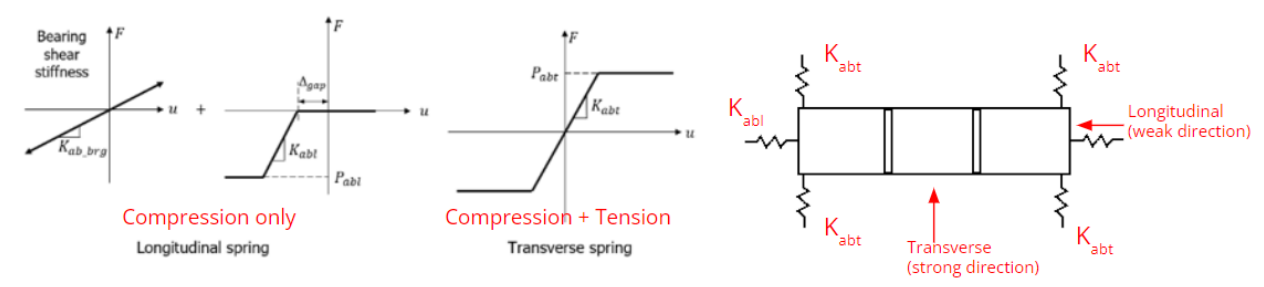
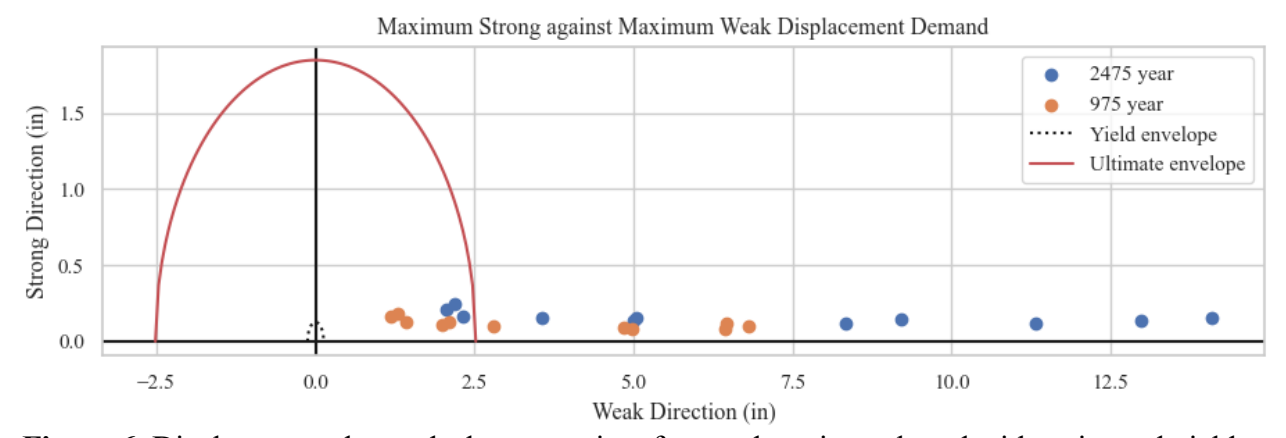


Figure 4. Idealized bilinear yield envelope used in analysis.



**Figure 5.** Simplified abutment spring models used in analysis. Based on (California Department of Transportation, 2019).



**Figure 6.** Displacement demands due to a suite of ground motions plotted with estimated yield envelopes.

### **Experimental Results**

A summary of the strong axis strengths is given in Table 2. Note that the effective yield load is estimated from a bilinear backbone curve and that drifts are calculated based on the displacement measured at the wall tip, about 7 feet up from the top of the footing and about 12 inches below the actuator attachment point. From the hysteresis plots in Figure 7, it can be seen that the presence of weak axis displacement causes strength loss at lower drift values and reduces the displacement capacity of the wall post peak strength. This is most substantial in test 3, where weak axis drift was increased up to 7.5% and drift at test conclusion was only around 2%, with the peak load only at around 85% of the previous two tests. However, the overall shape of the hysteresis until peak strength is similar between all three tests. In the weak direction, a larger ratio of weak axis to strong axis displacement resulted in higher strengths and better ductility in that direction, due to less damage accumulation from strong axis motion by that point. It is suggested that there is also a significant impact of the strong axis displacement history on the weak axis strength and ductility.

**Table 2.** Test Result Summary

	TWO I TO THE					
Specimen	Loading Protocol	Strong Axis				
		Peak load	Drift at effective	Drift at 80% of		
		(kips)	yield (%)	peak load (%)		
Wall 1	Uniaxial	276	0.5	2.5		
Wall 2	Bidirectional (4:1 ratio)	273	0.4	2.7		
Wall 3	Bidirectional (8:1 ratio)	238	0.3	2.2		

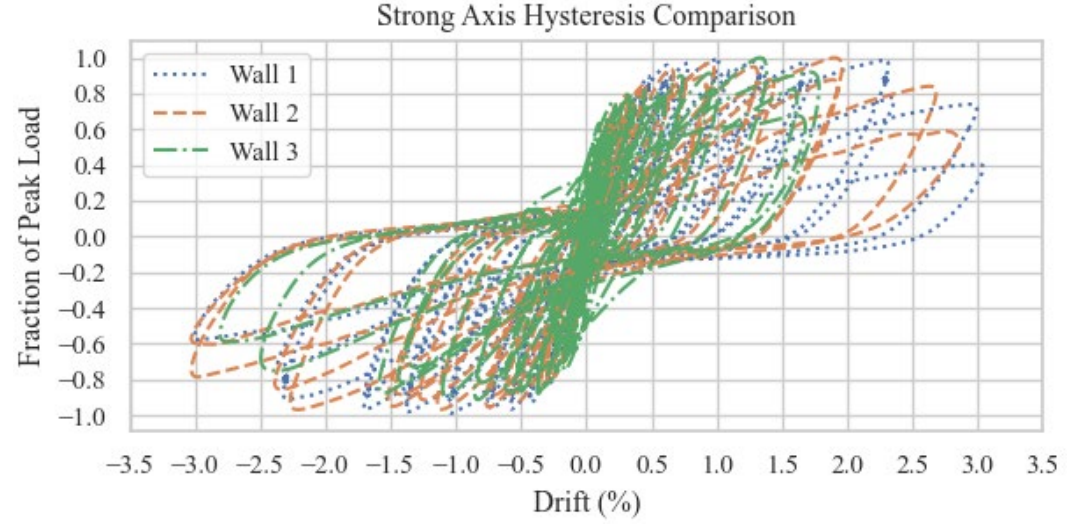


Figure 7. Strong axis force displacement hysteresis for all 3 wall tests.

# **Preliminary Conclusions**

Overall, all specimens were more ductile than initially thought, with the measured wall tip drift beyond 2% at the conclusion of the test. In the uniaxial test, and similarly for all three tests, initial horizontal flexure cracks appeared near the ends at the base of the wall and grew longer and new cracks formed higher up as the displacement targets increased. Then, diagonal cracks started to appear and became more inclined as the test progressed. These diagonal cracks joined together as the flexural cracks near the bottom edges grew.

All three walls experienced sliding shear failure, either at the wall-footing interface or at a horizontal crack in the plastic hinge. A final picture of the second specimen is shown in Figure 8. The formation of this failure plane is suggested as follows: after the vertical reinforcing bars yield near the ends due to flexure, the residual displacement caused the horizontal cracks to not fully close upon on load reversal. This was also seen as the displacement on the axial load jacks had to be decreased due to the wall elongating in the vertical direction. The large crack widths reduced the aggregate interlock shear force at the horizontal cracks. As the cracks propagated further and connected throughout the width of the wall, any spalled off or loose concrete acted to 'lubricate' the sliding interface, further leading to sliding motion. Once significant horizontal displacement in the strong axis was imposed, the yielded vertical bars started to kink and the entire wall displaced along the sliding plane. Due to lateral displacement along the sliding plane continuously yielding rather than fracturing the vertical bars, the wall strength was maintained

from about 0.5% to 2% drift, at which point the extreme vertical bars began to fracture and strength was lost.

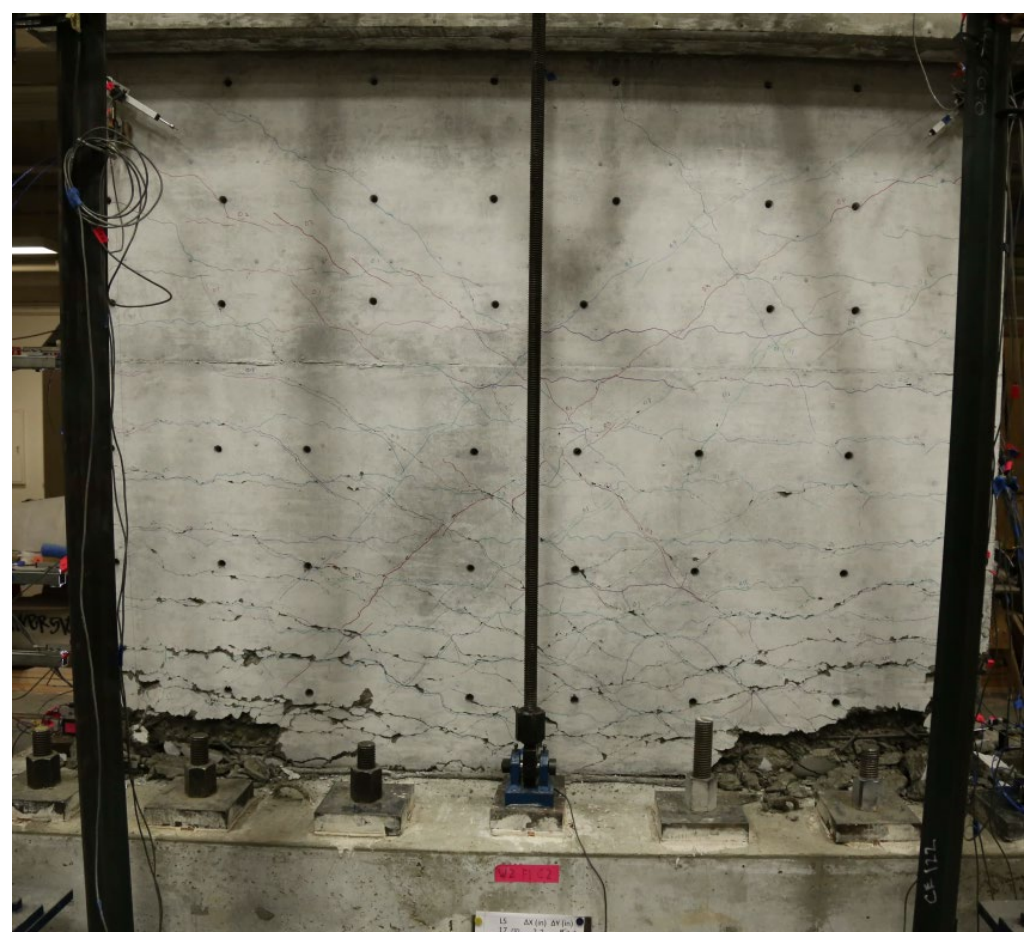


**Figure 8.** Final state of specimen 2. Horizontal and diagonal cracking patterns can be seen, along with spalling at the corners and large sliding cracks at the interface and near the base.

When weak axis displacement was added in the next two tests, the horizontal flexural cracks appeared sooner, mostly due to flexure action in the weak axis. Larger ratios of weak axis to strong axis displacement reduced the amount of diagonal shear cracks in favor of more horizontal flexural cracks. Yielding at the bottom bars due to the combination of weak axis and strong axis displacement also resulted in a similar sliding failure plane at the wall-footing interface. Weak axis displacement was also limited by the testing setup to 3% drift in test 2 and 7.5% drift in test 3.

### **CSMIP Data**

To better understand the relationship between the pier wall and global bridge behavior, two CSMIP instrumented pier wall bridges are being studied in further detail. The data recorded from these bridges (Center for Engeering Strong Motion Data) will help inform the displacement demands imposed on the pier walls and be used for model validation. The two chosen bridges are the Highway 101/Klamath River bridge (Figure 9) and the Highway 101/156 overpass (Figure

10). While the Klamath River bridge features a hollow reinforced concrete pier wall, the aspect ratio is closer to 2 and the shape of the wall is also not rectangular. In addition, there is no free-field sensor and there are sensors only at 3 of the bents with only one bent and abutment containing a complete set of sensors in all 3 orthogonal directions. On the other hand, the Highway 101/156 overpass bridge (henceforth referred to as the 156 bridge) has piers with aspect ratios below 1.0 and features a rectangular infill pier wall with typical Caltrans pier wall detailing. In addition, there are sensors at three different bents, a free field sensor, and a sensor at the bottom of one of the pier walls, which are useful to determine relative displacements and input ground motions. Thus, the 156 Bridge will be of initial focus.

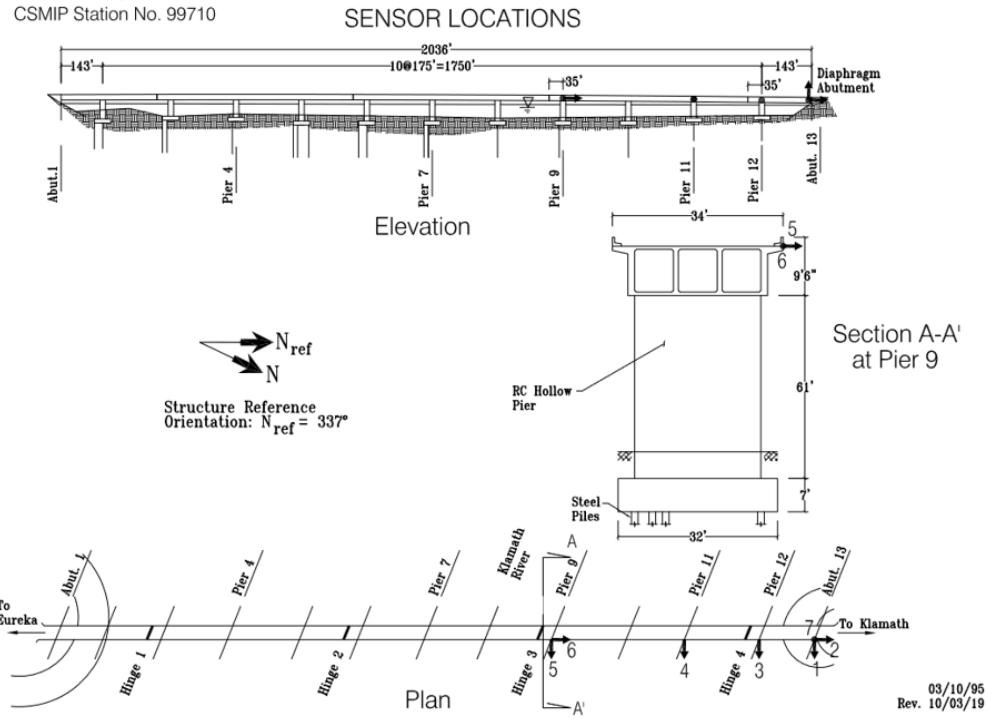


**Figure 9.** Sensor layout for Hwy101/Klamath River Bridge (Center for Engeering Strong Motion Data).

### 156 Bridge

The 156 bridge is a six-span bridge that originally had two columns per bent but was retrofitted in 2002 to include an infill wall. The bridge piers are 24 feet wide by 20 feet tall and 2 feet thick and has a skew of 34.8 degrees relative to the direction of travel. The reinforcement detailing of this infill wall is typical of Caltrans pier walls and of the first set of test specimens, namely uniform vertical reinforcement of #9 bars at 12", horizontal reinforcement of #5 bars @ 6" in the plastic hinge, and #5 crossties. The infill wall is connected to the existing piers and footings by drilled, bent steel dowels.

Sensor data is available for bents 3, 4, and 5 at the top of the bridge pier, with an additional sensor at the base of the bridge pier for bent 5, which is beneficial to determine relative displacements of the pier. There is also a free field set of sensors to serve as the basis

input ground motion. The available ground motions after the infill wall retrofit and their given peak accelerations are given in Table 3.

### Ground Motion Orbits at Bent 5

At bent 5, there are sensors both at the top and bottom of the pier wall. As a result, the relative displacement can be calculated and the orbits for the different ground motions are shown in Figure 11. The largest displacement measured was 0.12 cm in the pier weak direction and occurred in the Aromas 2007 event, while other motions displaced the structure less than 0.05 cm. Consequently, these ground motions did not deform the structure beyond the elastic range.

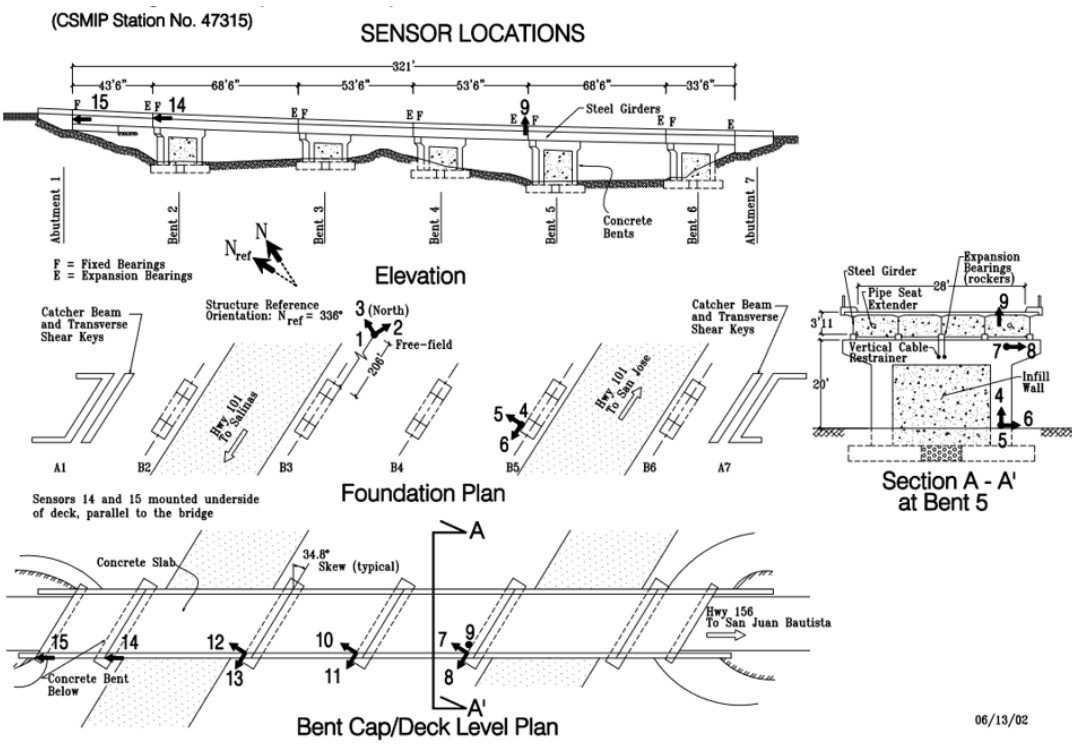
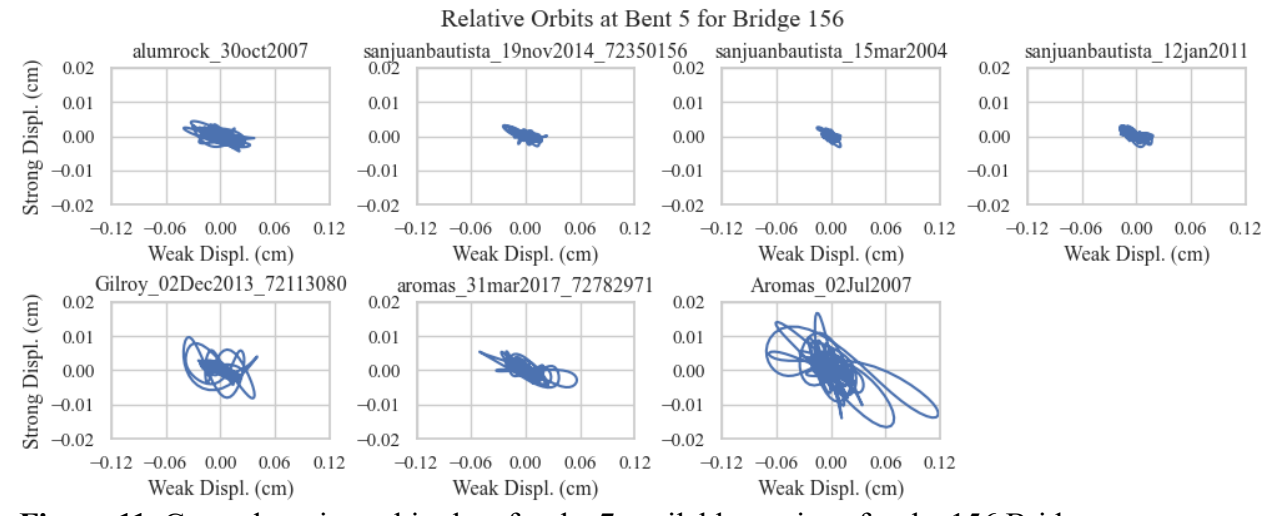


Figure 10. Sensor layout for Hwy101/156 Overpass (Center for Engeering Strong Motion Data).

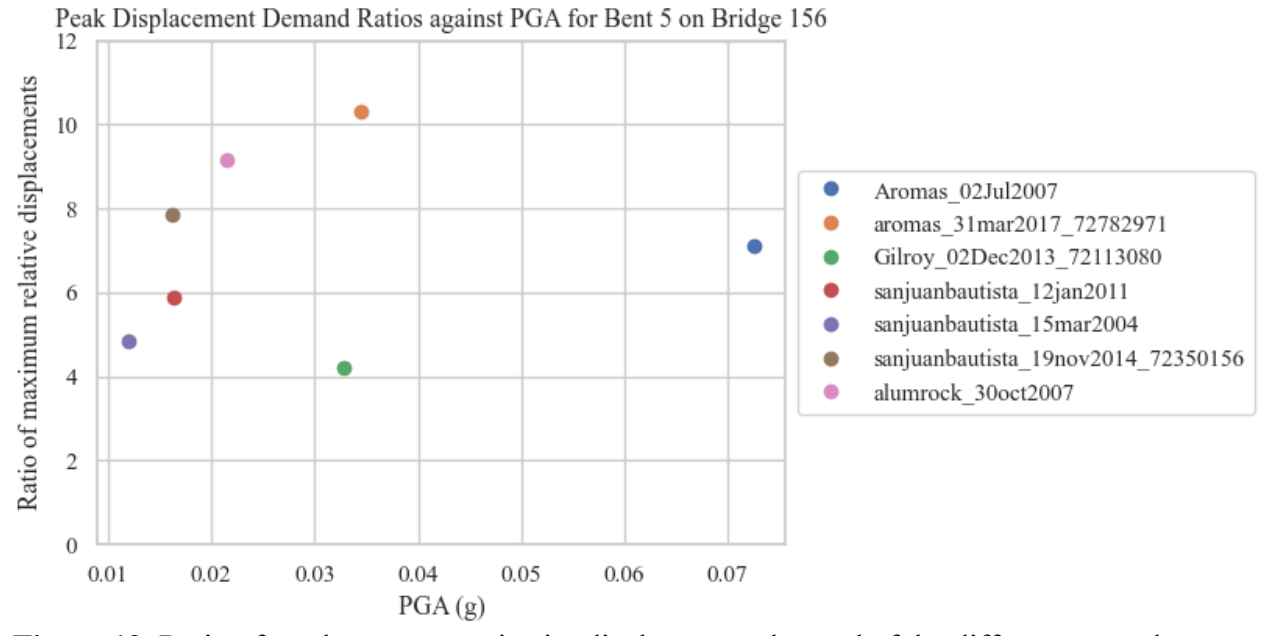
Due to the much lower weak axis stiffness of the wall, displacements are generally at least 4 times larger in that direction compared to the strong direction (Figure 12). This pattern is consistent for all the ground motions, despite the varying PGA of each event. The displacement demands are also quite small due to the limited number of motions with significant shaking. Nevertheless, the 4-10 times larger weak direction displacement demands than in that in the strong direction affirms the choice of bidirectional loading protocol in the second and third wall specimens, as analyzed previously with Bispec. There is no trend with displacement ratio with increasing PGA as the wall remains in the linear range for all motions, which can be seen by the relatively linear acceleration against displacement chart in Figure 13.

Table 3. Available Ground Motions for the 156 Bridge

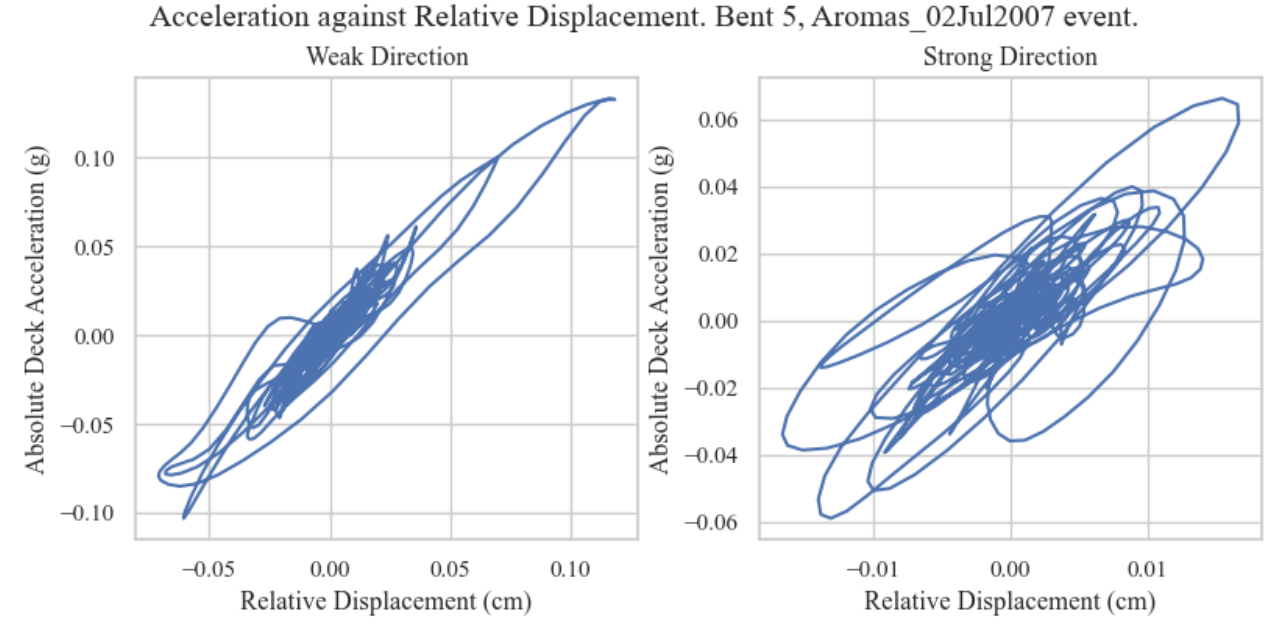
Event Name	PGA Ground (g)	PGA Structure (g)
alumrock_30oct2007	0.021	0.045
sanjuanbautista_19nov2014	0.016	0.027
sanjuanbautista_15mar2004	0.012	0.020
sanjuanbautista 12jan2011	0.016	0.026
Gilroy 02Dec2013	0.033	0.058
aromas 31mar2017	0.036	0.068
Aromas_02Jul2007	0.073	0.134



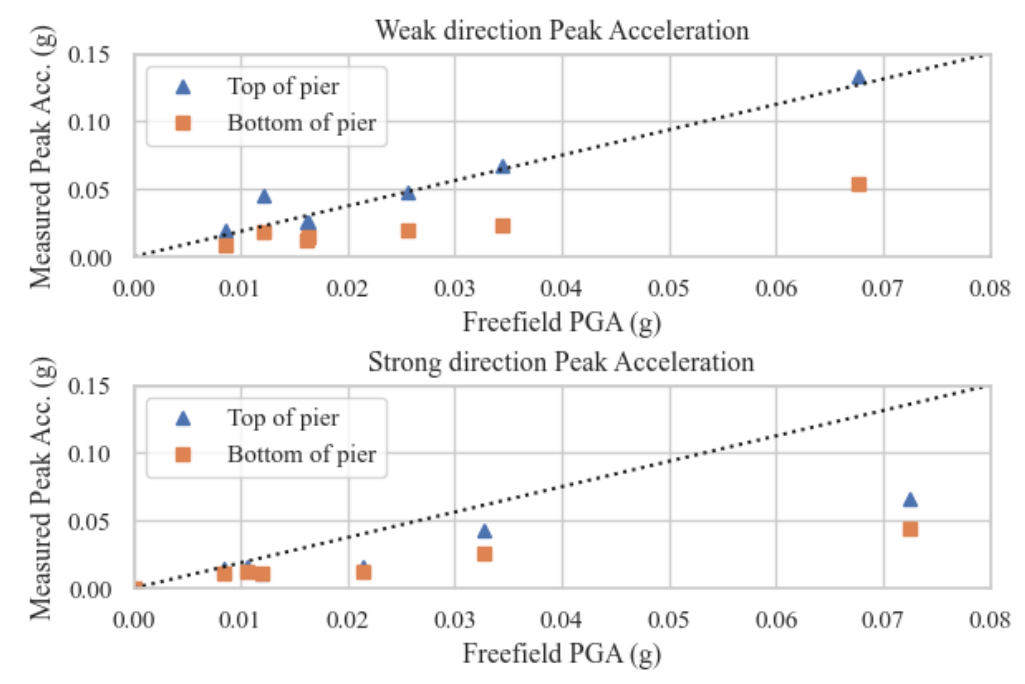
**Figure 11.** Ground motion orbit plots for the 7 available motions for the 156 Bridge.



**Figure 12.** Ratio of weak to strong axis pier displacement demand of the different ground motions.



**Figure 13.** Deck absolute acceleration against deck relative displacement for Bent 5. A linear force-displacement trend is seen.



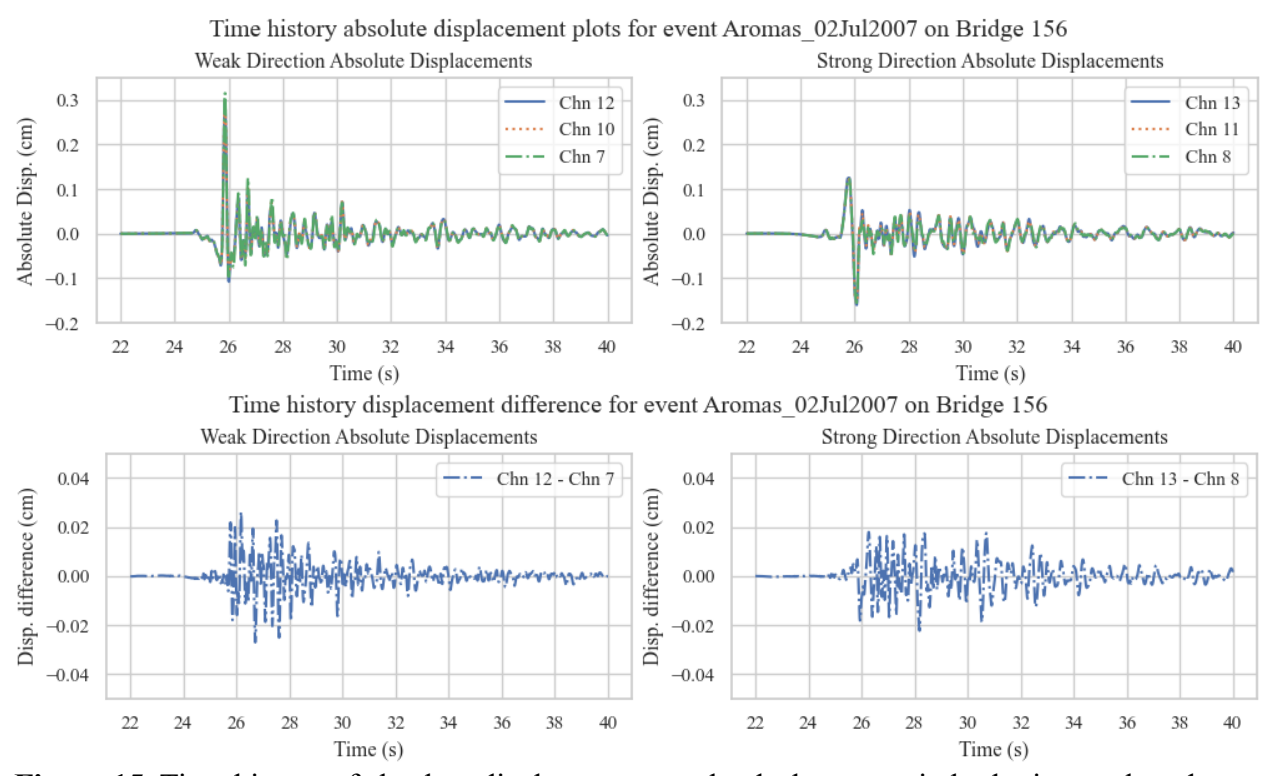
**Figure 14.** Peak acceleration at the top and bottom of the pier compared to the free field peak acceleration.

Figure 14 compares the measured peak acceleration at the top and bottom of the pier, in both directions, to the free field sensor data. It is noted that in all cases the peak acceleration at the top of the bent is greater than that measured at the base, indicating dynamic amplification from the pier wall and bridge system. This amplification is more pronounced in the weak direction, possibly because the natural frequency in the weak pier direction was closer to the

ground motion excitation period. Further, the peak acceleration at the base of the footing was consistently less than that measured at the free field.

### Aromas 2007 Motion

Although accurate relative displacements cannot be obtained for the other bents since there is no sensor at their bases, the absolute displacements can be plotted to observe the variation in the motion across the bridge deck. From the time history plots of three adjacent bents (bents 3, 4, and 5), little variation in the displacement time history is seen across the bridge (Figure 15). The maximum difference between bents 3 and 5 is on the order of 0.02 cm, while the two bents are approximately 32.6 meters apart. This indicates that, for the strongest recorded ground motion, there was negligible little torsion in the bridge, despite the skew of the bridge piers.



**Figure 15.** Time history of absolute displacements at the deck sensors in both pier weak and strong directions.

## **Conclusions**

Bidirectional testing on large scale squat pier wall specimens indicated that, with proper detailing and confinement in the plastic hinge region, along with a lower ratio of vertical reinforcement to reduce flexural strength, squat shear walls can have larger ductility than that typically expected. Sliding shear caused by the yielding and residual elongations of the vertical bars contributed significantly to the displacement capacity of the shear walls. The addition of bidirectional loading can reduce the strength and displacement capacity in both the strong and weak axis, indicating capacity interaction due to bidirectional loading.

Both initial modelling and CSMIP data analysis of a pier wall bridge indicates larger displacement demands in the weak direction than the strong direction by a factor of 4-10 times. Future work includes validating a component pier wall model based on experimental results before combining it with a global bridge model and using CSMIP data to validate initial behavior. However, due to the small PGAs available in the recorded ground motions, only data from the linear elastic portion of the pier walls is directly available. Thus, direct validation of non-linear behavior may be difficult.

#### References

- Abo-Shadi, N., Saiidi, M., & Sanders, D. (2000). Seismic Response of Reinforced Concrete Bridge Pier Walls in the Weak Direction. *University of Nevada*.
- California Department of Transportation. (2019). Caltrans Seismic Design Criteria Version 2.0. 6-22.
- Center for Engeering Strong Motion Data. (n.d.). *Strong-Motion Data Set*. Retrieved 2024, from https://www.strongmotioncenter.org/stationmap\_worldwide/all\_stations.php
- Earthquake Solutions. (n.d.). Bispec. Retrieved 2024, from https://eqsols.com/products/bispec/
- Gulec, C. K., & Whittaker, A. S. (2009). Performance-Based Assessment and Design of Squat Reinforced Concrete Shear Walls. Buffalo, New York: Technical Report MCEER-09-0010.
- Haroun, M. A., Pardoen, G. C., Shepherd, R., Haggag, H. A., & Kazanjy, R. P. (1994). Assessment of Cross-tie Performance in Bridge Pier Walls. *UC Irvine*.